Supplement of Atmos. Chem. Phys., 15, 7103–7125, 2015
http://www.atmos-chem-phys.net/15/7103/2015/
doi:10.5194/acp-15-7103-2015-supplement

Atmospheric Chemistry and Physics Open Access

Supplement of

Top-down constraints on atmospheric mercury emissions and implications for global biogeochemical cycling

S. Song et al.

Correspondence to: S. Song (song33@mit.edu)

A survey of laboratory studies for rate constants of dark oxidation of Hg_{aq}^0 (K_{OX2}):

Amyot et al. (1997) first showed that seawater Hg_{aq}^0 could undergo rapid oxidation in dark conditions. They collected seawater samples from the Gulf of Mexico, spiked them with known amounts of Hg_{aq}^0, and measured time series of Hg_{aq}^0 and total aqueous Hg. A first-order rate constant of (2.5-3.3) × 10^{-5} s^{-1} for dark oxidation was obtained. This rate was considered to be unreliable because other Hg_{aq}^0 loss pathways also existed, including volatilization from solution and adsorption on container wall. Using a similar method, Lalonde et al. (2001) indicated that the first-order reaction rate of dark oxidation in the Baie Saint-Paul river water was 1.7 × 10^{-5} s^{-1}. Lalonde et al. (2004) measured no significant loss of Hg_{aq}^0 under a dark environment. However, they observed dark oxidation of Hg_{aq}^0 (8.3 × 10^{-6} s^{-1}) if the natural water had been irradiated by ultraviolet light for 2 hours before being kept in the dark. Qureshi et al. (2010) proposed two possible redox pathways for surface ocean Hg. Both pathways included relatively high reaction rates of dark oxidation, i.e., (0.9-2.2) × 10^{-4} s^{-1} and (1.1-2.6) ×10^{-4} s^{-1}. They noted that the 2 dark oxidation rate constants were likely to be upper limits. In short, we find from these studies that the rate constants of dark oxidation (K_{OX2}) may range from 10^{-6} to 10^{-4} s^{-1}.

Table S1. Pearson's correlation coefficients based on hourly Hg^0 concentration data between the several AMNet sites, which are omitted from our inversion study. The bold number in each cell is the correlation coefficient (r), and the number below is the number of paired samples (n). Because of the strong correlations between these sites (r = 0.36-0.61, $n \approx 10^4$), only the site of KEJ is included in the inversion (see Table 1 of the main text). Locations of the other AMNet sites are: TPF (Thompson Farm, NH, USA; 43°N 71°W), UDH (Underhill, VT, USA; 45°N 73°W), PNR (Piney Reservoir, MD, USA; 40°N 79°W), and STW (Stiwell, OK, USA; 36°N 95°W).

	KEJ	TPF	UDH	PNR
TPF	**0.50** 8925			
UDH	**0.50** 9644	**0.59** 10231		
PNR	**0.47** 8948	**0.49** 9180	**0.61** 9980	
STW	**0.39** 7683	**0.36** 8095	**0.51** 8635	**0.50** 8157

Table S2. Pearson's correlation coefficients between different observational sites based on hourly Hg^0 concentration data. The bold number in each cell is the correlation coefficient (r), and the number below is the number of paired samples (n). Several sites, including MBO, CBS, WLG, NMC, SGR, LUL, NWN, and AMS, are not included in this table due to lack of hourly data. As shown in the table, these observational sites show relatively weak correlations ($-0.3 < r < 0.4$, $n = 10^3$-10^4).

	KEJ	YKV	GRB	HTW	ATS	SCZ	MLO	EGB	BRL	SAT	OKN	CPT	MHD	BKN	WLD	ZEP
YKV	**0.25** 6387															
GRB	**0.23** 6307	**0.15** 4723														
HTW	**0.24** 8185	**0.10** 6307	**0.14** 6100													
ATS	**0.27** 8908	**0.22** 6805	**0.23** 6550	**0.12** 8632												
SCZ	**0.10** 4673	**0.00** 3316	**0.04** 3488	**-0.08** 4104	**0.00** 4272											
MLO	**0.00** 2316	**0.06** 1423	**0.04** 1626	**0.09** 1935	**0.04** 2017	**0.04** 1523										
EGB	**0.05** 9335	**0.09** 7566	**-0.02** 6866	**0.08** 9496	**0.29** 10624	**0.14** 3980	N.A.									
BRL	**0.19** 8689	**0.17** 7125	**0.12** 6485	**0.04** 8897	**0.34** 10106	**0.07** 3893	N.A.	**0.27** 15271								
SAT	**0.25** 8072	**0.19** 6366	**0.14** 5752	**0.11** 7827	**0.22** 9006	**0.08** 3501	N.A.	**0.14** 13801	**0.24** 12916							
OKN	**-0.02** 8667	**-0.03** 6487	**-0.07** 6389	**-0.07** 8084	**-0.01** 9058	**0.04** 4710	**-0.00** 2253	**0.20** 9701	**0.11** 9226	**0.02** 8381						
CPT	**0.07** 13381	**-0.01** 10034	**0.04** 9871	**0.04** 12747	**0.08** 13982	**-0.07** 7079	**-0.03** 3314	**0.02** 15053	**0.03** 14271	**0.07** 12669	**-0.14** 13770					

MHD	**0.13** 12714	**0.06** 9661	**0.07** 9322	**-0.09** 12204	**0.10** 13517	**-0.07** 6484	**0.04** 2907	**-0.04** 14932	**0.05** 14100	**-0.03** 12723	**-0.00** 13165	**0.13** 20003				
BKN	**0.16** 6657	**-0.01** 4651	**0.12** 4875	**0.07** 5868	**0.26** 6197	**0.02** 5550	**0.19** 2570	**0.22** 4691	**0.22** 4759	**0.18** 3997	**-0.08** 6610	**0.09** 9788	**0.02** 9262			
WLD	**0.09** 10149	**0.06** 7566	**0.06** 7492	**0.02** 9707	**0.07** 10600	**0.01** 5166	**0.06** 2552	**-0.06** 11423	**0.01** 10731	**0.01** 9584	**-0.00** 10362	**-0.01** 15831	**0.03** 15104	**0.30** 7272		
ZEP	**0.05** 5871	**-0.01** 4525	**-0.09** 4430	**0.01** 5245	**-0.02** 6360	**-0.03** 2575	**-0.17** 1466	**0.08** 6489	**0.05** 6170	**-0.02** 4519	**-0.03** 6242	**-0.08** 9065	**0.05** 9374	**0.13** 4109	**0.10** 6990	
TRS	**0.22** 6114	**0.08** 4684	**0.10** 4612	**0.11** 6403	**0.06** 6686	**0.14** 3735	**0.18** 1298	**0.01** 7811	**0.18** 7645	**0.14** 7830	**-0.07** 6439	**0.01** 10091	**0.00** 9074	**0.18** 5117	**0.07** 7405	
ADY	**0.35** 3709	**0.25** 2863	**0.07** 2903	**-0.11** 3235	**0.16** 3837	**0.24** 2342	**0.10** 1356	**0.28** 2838	**0.29** 2821	**0.10** 2237	**0.09** 3974	**-0.05** (5747	**0.29** 5831	**0.14** 3752	**0.09** 4315	**0.23** 5963
ALT	**0.34** 1866	**0.36** 1348	**0.25** 1257	**0.36** 1659	**0.14** 2136	N.A.	N.A.	**-0.03** 3264	**-0.26** 3037	**0.03** 2022	**-0.02** 1913	**-0.06** 2902	**0.02** 2987	N.A.	**0.18** 2284	**0.17** 3219

N.A. = Not Available

Table S3. Summary of over-water mercury observational data in the North Atlantic Ocean.

Year	Month	Latitude	Method	Hg^0_{obs} [a]	Hg^0_{nor} [a]	Errors in observations[a]					Ref.[b]
						σ_{RE}	σ_{IP}	σ_{SF}	σ_{MM}	σ_{TOT}	
1990	Oct-Nov	7-54N	Manual	2.25	1.38	0.19	0.14	0.05	0.02	0.24	(1)
1993	Aug	50-68N	Manual	2.10	1.36	0.16	0.14	0.25	0.03	0.33	(2)
1994	Oct-Nov	6-54N	Manual	1.79	1.10	0.15	0.11	0.06	0.02	0.20	(1)
1996	Oct-Nov	8-67N	Tekran	2.12	1.52	0.13	0.15	0.06	0.02	0.21	(1)
1999	Sep	31-32N	Manual	2.03	1.57	0.10	0.16	0.12	0.02	0.22	(3)
1999	Dec	31-32N	Manual	2.06	1.60	0.10	0.16	0.80	0.04	0.82	(3)
1999	Dec	10-54N	Tekran	2.05	1.59	0.10	0.16	0.01	0.04	0.19	(1)
2000	Mar	31-32N	Manual	1.90	1.49	0.09	0.15	0.57	0.04	0.59	(3)
2003	Aug-Sep	10-37N	Tekran	1.63	1.35	0.06	0.14	0.01	0.03	0.15	(4)
2004	Jun-Aug	54-67N	Tekran	1.54	1.31	0.05	0.13	0.01	0.05	0.15	(5)
2005	Jul	60-62N	Tekran	1.78	1.60	0.04	0.16	0.00	0.05	0.17	(6)
2006	Aug	58-67N	Tekran	1.32	1.18	0.03	0.12	0.01	0.03	0.13	(7)
2007	Apr	43-59N	Tekran	2.26	2.17	0.02	0.22	0.02	0.04	0.22	(7)
2008	Nov	25-50N	Tekran	1.14	1.09	0.01	0.11	0.02	0.04	0.12	(8)
2008	Aug	35-45N	Tekran	1.40	1.35	0.01	0.14	0.02	0.03	0.14	(9)
2008	Sep	32-34N	Tekran	1.46	1.41	0.01	0.14	0.00	0.02	0.14	(9)
2009	Apr-May	25-50N	Tekran	1.15	1.15	0.00	0.12	0.02	0.04	0.12	(8)
2009	Jun	31-32N	Tekran	1.43	1.43	0.00	0.14	0.01	0.05	0.15	(9)
2009	Oct	35-45N	Tekran	1.40	1.40	0.00	0.14	0.02	0.02	0.14	(9)

[a]Unit for mercury concentrations is ng m^{-3}.

[b]References: (1) Temme et al. (2003); (2) Mason et al. (1998); (3) Mason et al. (2001); (4) Laurier and Mason (2007); (5) Aspmo et al. (2006); (6) Sommar et al. (2010); (7) Soerensen et al. (2010a); (8) Kuss et al. (2011); (9) Soerensen et al. (2013). Most of the above data has been summarized in Soerensen et al. (2012), Supporting material Table S1.

Table S4. Present-day reservoirs and fluxes used to calculate first-order rate coefficients in 7-box model of Hg global biogeochemical cycling. "Default" values are obtained from Table S2 in Amos et al. (2014), and the first and second simulations represent reference and optimized simulations, respectively. All fluxes are in Mg yr^{-1}.

	Default	1st simulation[a]	2nd simulation[a]
Atmosphere	5000 Mg	*4700 Mg*	*4400 Mg*
Hg^{II} deposition to land	1500	*1670*	*1620*
Hg^{0} deposition to land	1500	*1430*	*1320*
Hg^{II} deposition to ocean	3600	*4000*	*4000*
Hg^{0} air-sea exchange, gross loss to the ocean	1700	*1600*	*1500*
Surface ocean	2900	*3280 Mg*	*4100 Mg*
Hg^{0} air-sea exchange, gross evasion to atmosphere	4700	*4600*	*4800*
Particle settling to the subsurface ocean	3300	*2280*	*340*
Water transfer to subsurface ocean	5100	*5800*	*7300*
Subsurface ocean	130,000 Mg	*123,000 Mg*	*123,000 Mg*
Particle settling to the deep ocean	480	*460*	*460*
Water transfer to surface ocean	7100	*7000*	*7000*
Water transfer to deep ocean	340	*320*	*320*
Deep ocean	220,000 Mg	—	—
Burial to deep sediments	210	—	—
Water transfer to subsurface ocean	180	—	—
Fast terrestrial reservoir	9600 Mg	—	—
Evasion due to respiration of organic carbon[b]	45	*690*	*360*
Photochemical re-emission of deposited Hg	85	*1270*	*680*
Biomass Burning	290	*200*	*200*
Transfer to the slow pool	330	—	—
Transfer to the armored pool	10	—	—
Riverine discharge to ocean margins	710	—	—
Slow soil reservoir	35,000 Mg	—	—
Evasion due to respiration of organic carbon[b]	25	*370*	*200*
Biomass burning	8	*6*	*6*
Transfer to fast pool	210	—	—
Riverine discharge to ocean margins	20	—	—
Armored soil reservoir	190,000 Mg	—	—
Evasion due to respiration of organic carbon[b]	3	*37*	*20*
Biomass burning	4	*3*	*3*
Transfer to fast pool	15	—	—
Riverine discharge to ocean margins	10	—	—
External inputs		—	—
Geogenic emissions	90	—	—
Anthropogenic emissions	*f(t)*[c]	—	—
Anthropogenic discharges to rivers	*f(t)*[c]	—	—

[a]Italic values show changes of the 1st and 2nd simulations.
[b]In our simulation cases, the evasions from the soil reservoirs are larger than the default values in Amos et al. (2014).
[c]A function of time as shown in Amos et al. (2014).

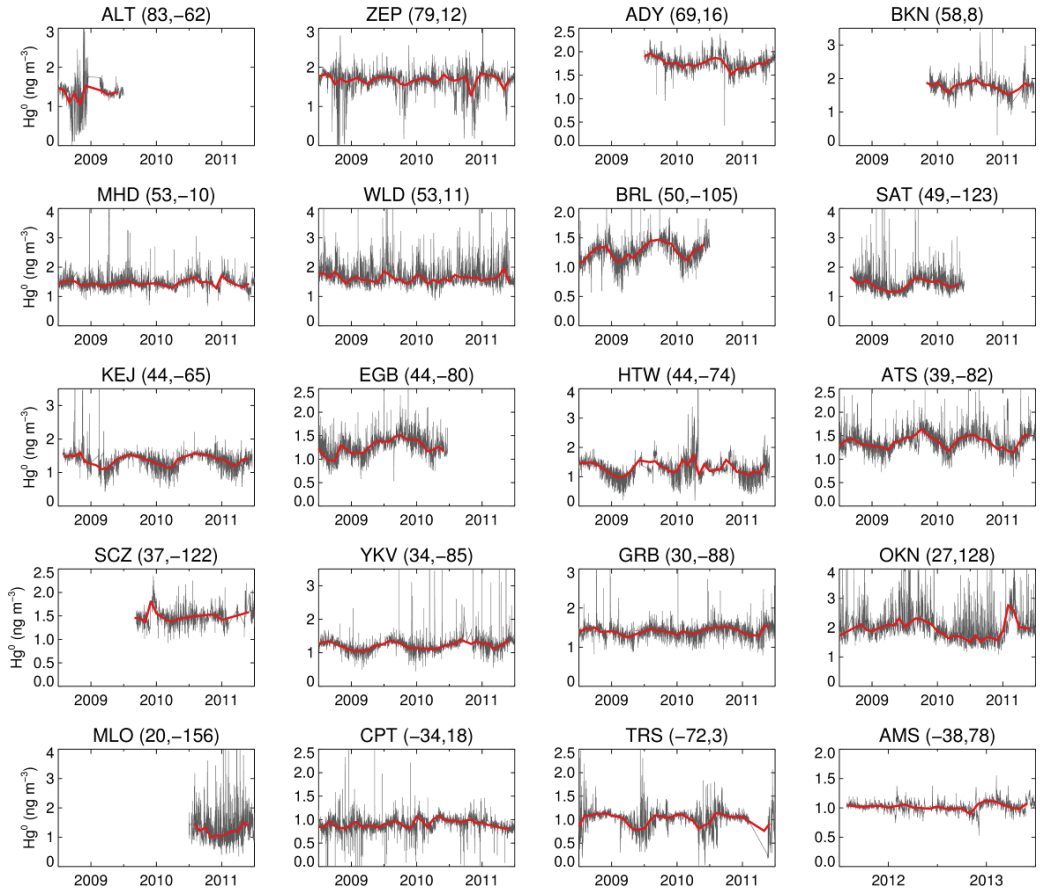

Fig. S1. Hourly (grey) and monthly (red) Hg^0 concentrations measured at ground-based sites. Note different scales on vertical axes.

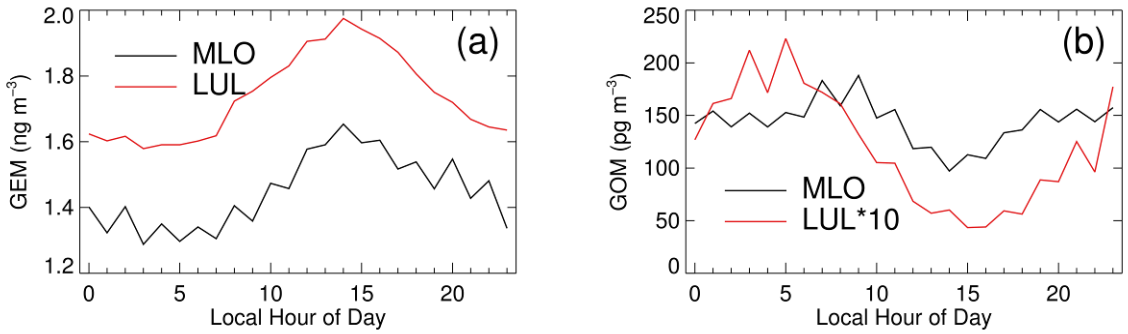

Fig. S2. Diurnal variations of the average GEM (panel a) and GOM (panel b) concentrations measured at two mountain sites, Mauna Loa (MLO) and Mt. Lulin (LUL). Data for LUL are from Fig. 3 of Sheu et al. (2010). From panel (a) we estimate, for both sites, that the minimum hourly Hg^0 concentration in the nighttime is ~ 90% of the all-day average.

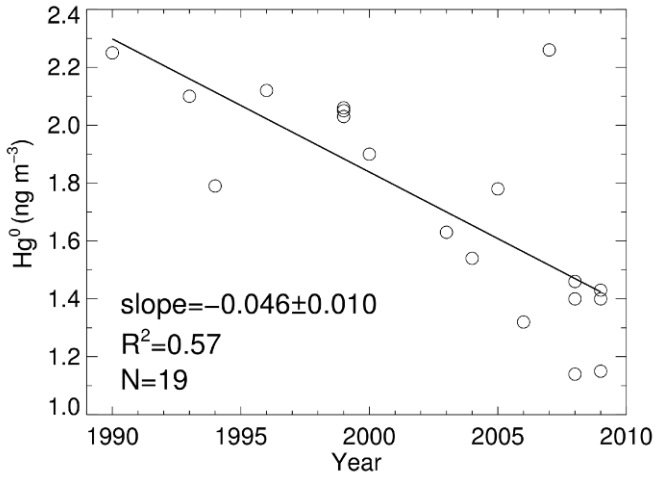

Fig. S3. Multi-decadal decline trend of Hg^0 concentration calculated from 19 ship cruise measurements in 1990-2009. The slope of -0.046 ± 0.010 ng m^{-3} yr^{-1} is used to normalize all observed data (Hg^0_{obs}) to the concentration level of the year 2009 (Hg^0_{nor}).

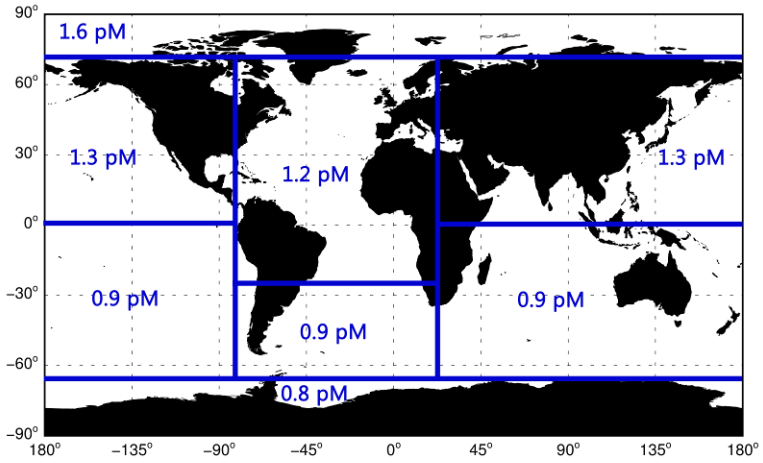

Fig. S4. Subsurface water concentrations of inorganic mercury used in this study. These basin-specific data are compiled by Soerensen et al. (2010b) and updated based on new measurements. The Hg concentration in the North Atlantic Ocean (NAO) is reduced from 1.8-2.0 pM to 1.2 pM, according to the vertical profiles measured at the Bermuda Atlantic Time Series (BATS, 31°40'N 64°10'W) in June 2008 (Lamborg et al., 2012). Mercury concentration in the South Atlantic Ocean (SAO) is reduced to 0.9 pM, at the low end of uncertainty range by Sunderland and Mason (2007). The southern boundary of the North Pacific (NP), where mercury concentration is set as 1.3 pM, is extended to the equator since Munson (2014) measured total mercury concentration of 1-1.5 pM in the Tropical Pacific Ocean.

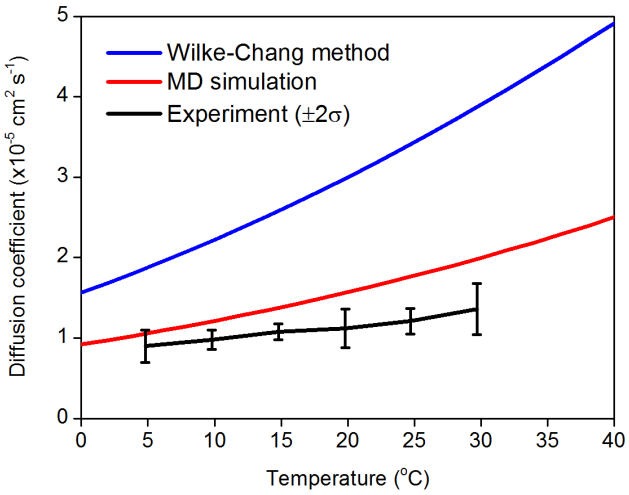

Fig. S5. Comparison of the Hg^0 diffusion coefficients (D_{Hg}) in seawater determined by the Wilke-Chang method (Wilke and Chang, 1955), MD (molecular dynamics) simulation (Kuss et al., 2009), and the laboratory experiment (Kuss, 2014). The Wilke-Chang method can be found in Soerensen et al. (2010b). The parameterization of the MD simulation is D_{Hg} (cm^2 s^{-1}) = 0.02293 × $e^{(17.76\ kJ/mol)/RT}$, with R the gas constant and T the temperature in K.

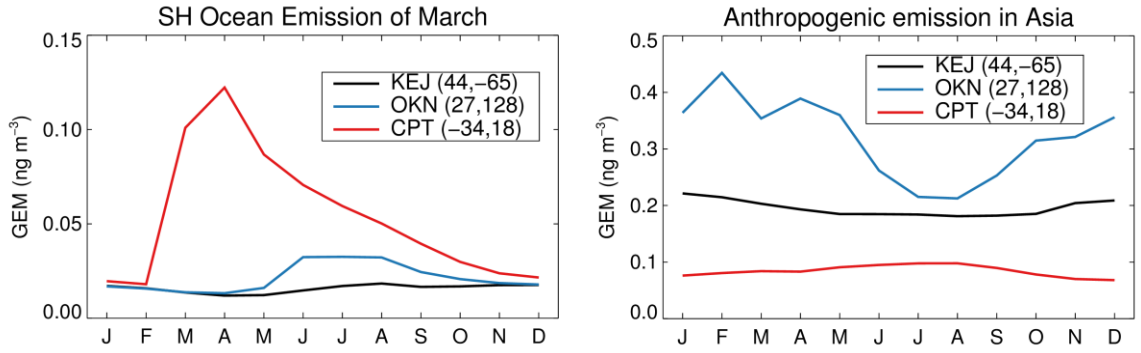

Fig. S6. Sensitivities of monthly Hg^0 concentrations at 3 ground-based observational sites to changes in different sources: (left) the SH ocean emission in March and (right) anthropogenic emission in Asia. The SH ocean emission in March has larger sensitivities in the SH site CPT than the two NH sites (KEJ and OKN). The sensitivities at CPT exhibit an exponential decay starting from March-April. The anthropogenic emission in Asia has the largest sensitivities in OKN, which is located in the Asia-Pacific region. The smallest sensitivities are found for the SH site CPT because the Asian emissions are predominantly from the NH.

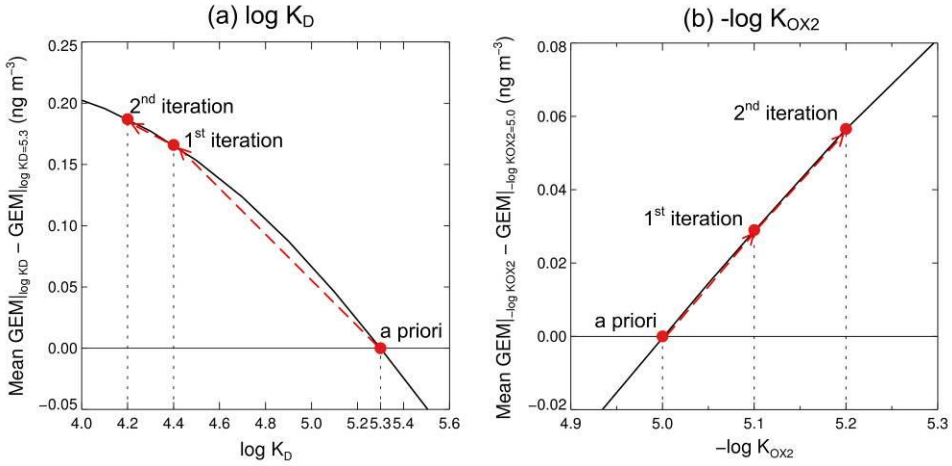

Fig. S7. Responses of Hg^0 concentrations to changes of the partition coefficient (log K_D) (panel a) and dark oxidation rate constant (-log K_{OX2}) (panel b). We also show in the figure the evolution of the two parameters from the *a priori* to *a posterior* estimate.

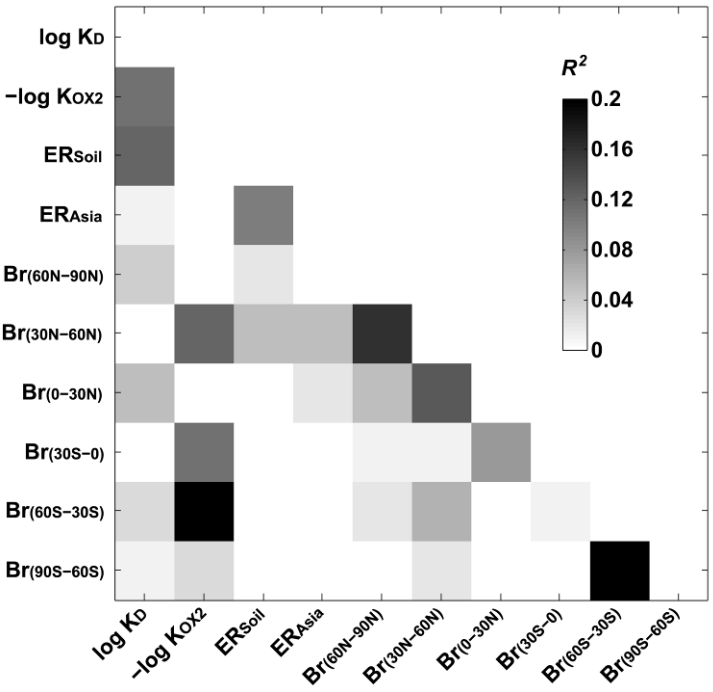

Fig. S8. Average correlations (R^2) between the optimized parameters derived from the special case of parameter inversion. Diagonal elements (identically equal to 1) are set to 0 for clarity. Each of the 6 bromine elements represents Br columns in a 30° latitudinal band, e.g., "$Br_{(60N-90N)}$" is the Br column from 60N to 90N. In this parameter inversion, we assume that each Br column has a one-sigma uncertainty of 50% and that its best estimate is the current value in GEOS-Chem.

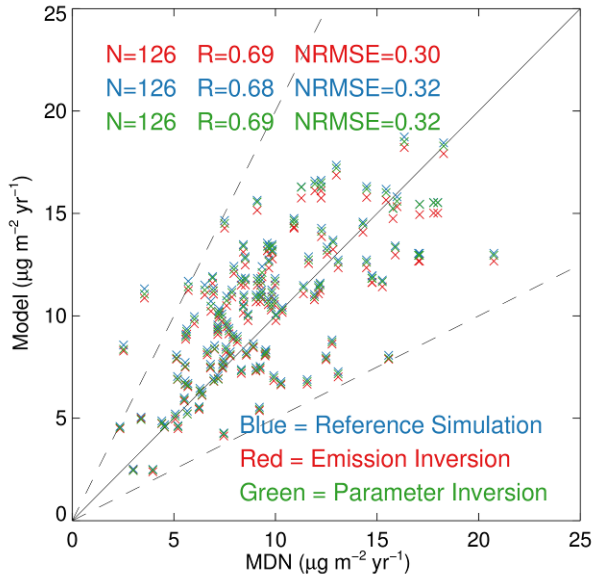

Fig. S9. Scatter plot comparing model outputs (reference simulation, emission inversion, and parameter inversion) to observations of mercury wet deposition fluxes from the NADP/MDN monitoring network during 2009-2011 (NADP/MDN, 2012). The selection criteria of the observational data have been described in Holmes et al. (2010). The solid line indicates the 1:1 ratio and the two dashed lines correspond to the deviation factors of 0.5 and 2.

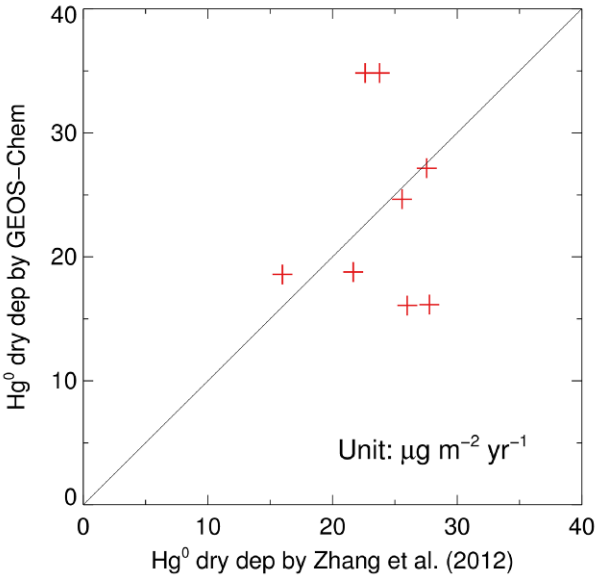

Fig. S10. Scatter plot (red plus sign) of annual Hg^0 dry deposition fluxes modeled by GEOS-Chem (reference simulation) and determined by Zhang et al. (2012). The solid line indicates 1:1 line. We calculate that the annual Hg^0 dry deposition fluxes from GEOS-Chem and Zhang et al. (2012) are both 24 μg m^{-2} yr^{-1}.

References

Amos, H. M., Jacob, D. J., Kocman, D., Horowitz, H. M., Zhang, Y., Dutkiewicz, S., Horvat, M., Corbitt, E. S., Krabbenhoft, D. P., and Sunderland, E. M.: Global biogeochemical implications of mercury discharges from rivers and sediment burial, Environ. Sci. Technol., 48, 9514-9522, doi:10.1021/es502134t, 2014.

Amyot, M., Gill, G. A., and Morel, F. M. M.: Production and loss of dissolved gaseous mercury in coastal seawater, Environ. Sci. Technol., 31, 3606-3611, doi:10.1021/es9703685, 1997.

Aspmo, K., Temme, C., Berg, T., Ferrari, C., Gauchard, P.-A., Fain, X., and Wibetoe, G.: Mercury in the atmosphere, snow and melt water ponds in the North Atlantic Ocean during Arctic summer, Environ. Sci. Technol., 40, 4083-4089, doi:10.1021/es052117z, 2006.

Holmes, C. D., Jacob, D. J., Corbitt, E. S., Mao, J., Yang, X., Talbot, R., and Slemr, F.: Global atmospheric model for mercury including oxidation by bromine atoms, Atmos. Chem. Phys., 10, 12037-12057, doi:10.5194/acp-10-12037-2010, 2010.

Kuss, J., Holzmann, J., and Ludwig, R.: An elemental mercury diffusion coefficient for natural waters determined by molecular dynamics simulation, Environ. Sci. Technol., 43, 3183-3186, doi:10.1021/es8034889, 2009.

Kuss, J., Zülicke, C., Pohl, C., and Schneider, B.: Atlantic mercury emission determined from continuous analysis of the elemental mercury sea-air concentration difference within transects between 50°N and 50°S, Global Biogeochem. Cy., 25, GB3021, doi:10.1029/2010gb003998, 2011.

Kuss, J.: Water–air gas exchange of elemental mercury: An experimentally determined mercury diffusion coefficient for Hg^0 water–air flux calculations, Limnol. Oceanogr., 59, 1461-1467, doi:10.4319/lo.2014.59.5.1461, 2014.

Lalonde, J. D., Amyot, M., Kraepiel, A. M. L., and Morel, F. M. M.: Photooxidation of Hg(0) in artificial and natural waters, Environ. Sci. Technol., 35, 1367-1372, doi:10.1021/es001408z, 2001.

Lalonde, J. D., Amyot, M., Orvoine, J., Morel, F. M. M., Auclair, J.-C., and Ariya, P. A.: Photoinduced oxidation of Hg^0(aq) in the waters from the St. Lawrence Estuary, Environ. Sci. Technol., 38, 508-514, doi:10.1021/es034394g, 2004.

Lamborg, C. H., Hammerschmidt, C. R., Gill, G. A., Mason, R. P., and Gichuki, S.: An intercomparison of procedures for the determination of total mercury in seawater and recommendations regarding mercury speciation during GEOTRACES cruises, Limnol. Oceanogr. Methods, 10, 90-100, doi:10.4319/lom.2012.10.90, 2012.

Laurier, F., and Mason, R.: Mercury concentration and speciation in the coastal and open ocean boundary layer, J. Geophys. Res.-Atmos., 112, D06302, doi:10.1029/2006jd007320, 2007.

Mason, R. P., Rolfhus, K. R., and Fitzgerald, W. F.: Mercury in the North Atlantic, Mar. Chem., 61, 37-53, doi:10.1016/S0304-4203(98)00006-1, 1998.

Mason, R. P., Lawson, N. M., and Sheu, G. R.: Mercury in the Atlantic Ocean: factors controlling air–sea exchange of mercury and its distribution in the upper waters, Deep-Sea Res. Pt. II, 48, 2829-2853, doi:10.1016/S0967-0645(01)00020-0, 2001.

Munson, K. M.: Transformations of mercury in the marine water column, Ph.D. Thesis, Joint Program in Oceanography (Massachusetts Institute of Technology, Department of Earth, Atmospheric, and Planetary Sciences; and the Woods Hole Oceanographic Institution), available at: http://hdl.handle.net/1721.1/87513, 2014.

NADP/MDN: Mercury Deposition Network, National Atmospheric Deposition Program, available at: http://nadp.sws.uiuc.edu/mdn/, 2012.

Qureshi, A., O'Driscoll, N. J., MacLeod, M., Neuhold, Y.-M., and Hungerbühler, K.: Photoreactions of mercury in surface ocean water: gross reaction kinetics and possible pathways, Environ. Sci. Technol., 44, 644-649, doi:10.1021/es9012728, 2010.

Sheu, G.-R., Lin, N.-H., Wang, J.-L., Lee, C.-T., Ou Yang, C.-F., and Wang, S.-H.: Temporal distribution and potential sources of atmospheric mercury measured at a high-elevation background station in Taiwan, Atmos. Environ., 44, 2393-2400, doi:10.1016/j.atmosenv.2010.04.009, 2010.

Soerensen, A. L., Skov, H., Jacob, D. J., Soerensen, B. T., and Johnson, M. S.: Global concentrations of gaseous elemental mercury and reactive gaseous mercury in the marine boundary layer, Environ. Sci. Technol., 44, 7425-7430, doi:10.1021/es903839n, 2010a.

Soerensen, A. L., Sunderland, E. M., Holmes, C. D., Jacob, D. J., Yantosca, R. M., Skov, H., Christensen, J. H., Strode, S. A., and Mason, R. P.: An improved global model for air-sea

exchange of mercury: high concentrations over the North Atlantic, Environ. Sci. Technol., 44, 8574-8580, doi:10.1021/es102032g, 2010b.

Soerensen, A. L., Jacob, D. J., Streets, D. G., Witt, M. L. I., Ebinghaus, R., Mason, R. P., Andersson, M., and Sunderland, E. M.: Multi-decadal decline of mercury in the North Atlantic atmosphere explained by changing subsurface seawater concentrations, Geophys. Res. Lett., 39, L21810, doi:10.1029/2012gl053736, 2012.

Soerensen, A. L., Mason, R. P., Balcom, P. H., and Sunderland, E. M.: Drivers of surface ocean mercury concentrations and air–sea exchange in the West Atlantic Ocean, Environ. Sci. Technol., 47, 7757-7765, doi:10.1021/es401354q, 2013.

Sommar, J., Andersson, M. E., and Jacobi, H. W.: Circumpolar measurements of speciated mercury, ozone and carbon monoxide in the boundary layer of the Arctic Ocean, Atmos. Chem. Phys., 10, 5031-5045, doi:10.5194/acp-10-5031-2010, 2010.

Sunderland, E. M., and Mason, R. P.: Human impacts on open ocean mercury concentrations, Global Biogeochem. Cy., 21, GB4022, doi:10.1029/2006gb002876, 2007.

Temme, C., Slemr, F., Ebinghaus, R., and Einax, J. W.: Distribution of mercury over the Atlantic Ocean in 1996 and 1999–2001, Atmos. Environ., 37, 1889-1897, doi:10.1016/S1352-2310(03)00069-4, 2003.

Wilke, C. R., and Chang, P.: Correlation of diffusion coefficients in dilute solutions, AIChE Journal, 1, 264-270, doi:10.1002/aic.690010222, 1955.

Zhang, L., Blanchard, P., Gay, D. A., Prestbo, E. M., Risch, M. R., Johnson, D., Narayan, J., Zsolway, R., Holsen, T. M., Miller, E. K., Castro, M. S., Graydon, J. A., Louis, V. L. S., and Dalziel, J.: Estimation of speciated and total mercury dry deposition at monitoring locations in eastern and central North America, Atmos. Chem. Phys., 12, 4327-4340, doi:10.5194/acp-12-4327-2012, 2012.